



Coefficient Adaptation Method for the Zwart Model

W. Jin¹, X. Xu^{1,2†}, Y. Tang¹, H. Zhou³, H. Zhou¹ and X. Ren^{1,2}

¹ State Key Laboratory of High Performance Computing, College of Computer, National University of Defense Technology, Changsha 410073, China

² Artificial Intelligence Research Center (AIRC), National Innovation Institute of Defense Technology (NIIDT), Beijing 100000, China

³ College of Aerospace Science and Engineering, National University of Defense Technology, Changsha 410073, China

†Corresponding Author Email: xuxinhai@nudt.edu.cn

(Received January 15, 2018; accepted July 3, 2018)

ABSTRACT

The coefficient adaptation problem is often encountered in CFD simulations. The accuracy of simulation results depends much on the empirical coefficients of mathematical models. Cavitation simulation is a typical application of CFD. Researchers have proposed methods to optimize the empirical coefficients of the cavitation model. However, these methods can only acquire constant values which aren't adaptive to all the operating conditions. This paper focused on the condensation and the evaporation coefficients of the Zwart model and considered quasi-steady cavitating flows around a 2-D NACA66(MOD) hydrofoil. For the first time, we gave a formal description of the coefficient adaptation problem, and put forward a method to model the relationship between the best coefficient values and the operating conditions. We designed and implemented the coefficient adaptation platform combining OpenFOAM, and validated the best coefficient values predicted by our method. The overall results show the predicted coefficient values result in an increase of accuracy by 12% in average, compared with the default values and the tuned values by Morgut, thus indicating our method can effectively solve the coefficient adaptation problem for the Zwart model. We believe the proposed method can be extended to other mathematical models in practical uses.

Keywords: Coefficient optimization; Zwart model; OpenFOAM; Cavitation; CFD.

1. INTRODUCTION

Cavitation is the phenomenon that occurs inside a liquid medium or on the surface of liquid and solid medium with the process of formation, development and collapse of cavities(or bubbles). It is commonly observed inside or on the surface of fluid machinery such as water airfoils, hydraulic turbines, pumps and marine propellers. Due to the geometry of the system, cavitation appears in low pressure regions of the flowing liquids where local pressure drops below a certain threshold value. In these examples, the occurrence of cavitation is undesirable because it usually leads to negative effects such as vibration, noise and material erosion (Brennen 1995; Franc and Michel 2005). It is critical to study the mechanism of cavitation in order to reduce the losses in industrial applications.

With the fast development of computer techniques in the last few decades, CFD (Computational Fluid Dynamics) methods have been playing an increasingly important role in investigating

cavitation because of less consumption of both time and resources compared to physical experiments. To describe the process of cavitation, researchers have developed numerous cavitation models, which can be divided into two categories, namely interface tracking models (Hirschi, Dupont, Avellan, Favre, Guelich, Handloser, and Parkinson 1998; Senocak and Wei 2004) and homogeneous equilibrium models (Merkle, Feng, and Buelow 1998; Kunz, Boger, Stinebring, Chyczewski, Lindau, Gibeling, Venkateswaran, and Govindan 2000; Schnerr 2001; Singhal, Athavale, Li, and Jiang 2002; Philip J. Zwart 2004). The former models are limited to two-dimensional planar or axisymmetric flows and difficult with three-dimensional simulation. The latter assume cavitating flows to be homogeneous and isothermal and solve the variation of the mixture density in the multiphase flow using a barotropic equation of state or a transport equation. However, barotropic equation of state cannot capture the dynamics of unsteady cavitating flows (Senocak and Shyy 2002); on the contrary, applying transport equations can simulate both steady and

unsteady cavitating flows. In the approach of transport equation models, an additional transport equation for either the mass or volume fraction of vapor with source terms to regulate the mass transfer between the two phases is solved. In the past decades, numerous transport equation models were proposed such as the Merkle model (Merkle, Feng, and Buelow 1998), the Kunz model (Kunz, Boger, Stinebring, Chyczewski, Lindau, Gibelung, Venkateswaran, and Govindan 2000), the Schnerr-Sauer model (Schnerr 2001), the Singhal model (Singhal, Athavale, Li, and Jiang 2002), the Zwart model (Philip J. Zwart 2004) and etc. They take into account different aspects of cavitating flows and imply different equations with evaporation and condensation rates to describe phase change. Most of these models include tunable parameters such as the condensation coefficient and the evaporation coefficient. Among them, the Zwart model has been integrated into commercial softwares such as ANSYS-CFX and fluent and widely used in simulating cavitating flows because of its effectiveness and stability (Philip J. Zwart 2004; Hagar Alm, Zhang, and Medhat 2012; Hou-lin, WANG, Deng-hao, Wei-min, and Ming-gao 2012).

The empirical coefficients of the cavitation models will affect the accuracy of simulation. Although default values of the coefficients are usually provided, they cannot always result in desirable simulation results. Thus, optimization of the empirical coefficients has to be performed. In recent years, researchers have investigated how to acquire better coefficient values. Hou-lin Liu *et al.* tested the value of each one of the four empirical coefficients of Zwart model by different orders of magnitude while setting the other three coefficients by default (Liu, Wang, Wang, Zhang, and Huang 2014). The results indicate the influence of each coefficient and the best order of magnitude for precise prediction. Morgut *et al.* tuned the empirical coefficients of the Zwart model, the Singhal model and the Kunz model respectively based on the simulation of the cavitating flow around the NACA66 (MOD) hydrofoil, using an optimization strategy driven by the modeFRONTIER optimization system, where three different cavitating flow regimes (different cavitation numbers) at the angle of attack of 4° were considered (Morgut, Nobile, Bilu, and Scaron 2011). The tuned coefficients agreed relatively well with the corresponding experiments of the three regimes and were then applied in the prediction of other flow regimes related to the NACA66 (MOD) hydrofoil. Surrogate-based optimization was also applied by some researchers to calibrate the coefficients in the simulation of some cavitating flows (Tushar, Siddharth, Haftka, Wei, and Zhao 2010; Zhao, Huang, Chen, Wang, Gao, and Zhao 2017). In literature efforts were made for the purpose of obtaining fixed values of the empirical coefficients that may generally go well with simulations under different operating conditions and even in new flow systems. It should be noted that fixed values cannot always perform well when operating conditions change. Meanwhile, in practical engineering, using traditional optimization

method to find the best coefficient values will consume lots of time and resources. The above issues generate demand for efficient and intelligent coefficient recommendation methods that help with the prediction of the best coefficient values adapted to certain operating conditions. It is of great significance to discover the relationship between the best coefficient values and the operating conditions using intelligent methods when more and more experimental measurements under different operating conditions have been acquired.

Besides the cavitation model, the turbulence model also plays an important role in cavitation simulations. In literature, two common categories of the turbulence model have been proposed, namely Boussinesq-based eddy viscosity models and Reynolds stress models. The former category includes the zero-equation model, the Spalart-Allmaras model and the two-equation models. The other category introduces a control equation of second order pulsation to form the second order moment closed model (Wilcox 1993). In actual engineering, the Spalart-Allmaras model and the two-equation turbulence models are widely used. These models can save computation time as well as produce simulation results which meet with engineering requirements. Among these models, the standard $k - \epsilon$ model (Launder and Spalding 1974) is one of the earliest two-equation turbulence models. It has been proved to have good performance in simulating the steady-state cavitating flows around the two-dimensional NACA66(MOD) hydrofoil (Singhal, Athavale, Li, and Jiang 2002; Morgut, Nobile, Bilu, and Scaron 2011).

Aiming at the issue mentioned above, we focused on the Zwart model and carried out research into the prediction of the best values of empirical coefficients, considering quasi-steady cavitating flows around a two-dimensional NACA66 (MOD) hydrofoil. For the first time, we give a formal description of the coefficient adaptation problem and solution. We put forward the coefficient adaptation model and corresponding method including two key modules: the optimization module and the prediction module, which can model relationship between the best coefficient values and the operating condition-s. We designed and implemented the coefficient adaptation platform for the Zwart model through the method mentioned above, combining the open source software OpenFOAM. Then we performed optimization of the condensation coefficient F_c and the evaporation coefficient F_e of the Zwart model and validated the predicted optimal coefficient values on the platform. The overall results indicate that our method can effectively solve the coefficient adaptation problem of the Zwart model and guide the configuration of the empirical coefficients under specific operating conditions.

It should be noted that our coefficient adaptation method is not limited to the Zwart model, but can be extended to other cavitation models or even other CFD models with empirical coefficients.

In the following, the formal description of coefficient adaptation problem is presented first, followed by the CFD models used in our simulations. Then the coefficient adaptation model for the Zwart model and the corresponding method are described. The experiments and numerical results are reported followed by our concluding remarks.

2. FORMAL DESCRIPTION OF COEFFICIENT ADAPTATION PROBLEM

The coefficient adaptation problem is that for the simulation of a specific flow case, how to decide the best values of empirical coefficients making the simulation results in best agreement with the experimental data for different operating conditions. Before giving our coefficient adaptation method, we present the formal description of the coefficient adaptation problem. For a specific flow case *Case*, let *D* denote the calculating domain, *M* the mathematical models used to describe the flow, *N* the numerical methods involved in the simulation, *I* the initial conditions of the simulation, then the simulation results can be defined as:

$$Sim_{Case}(D, M, N, I) \tag{1}$$

The initial conditions include the operating conditions and other initial settings. In later context, we replace *I* with *O* expressing the attention we pay to the operating conditions and neglect of other initial settings of the initial conditions. *M* consists of several mathematical equations, each of them containing none or several empirical coefficients. Let the empirical coefficients be the independent variables, then the equations may take the form as:

$$\begin{cases} Formula_1(c_{11}, \dots, c_{1p_1}) = 0 \\ Formula_2(c_{21}, \dots, c_{2p_2}) = 0 \\ \vdots \\ Formula_m(c_{m1}, \dots, c_{mp_m}) = 0 \end{cases} \tag{2}$$

Here, c_{i1}, \dots, c_{ip_i} are the empirical coefficients in the *i*th equation, and $p_i \geq 0$ ($i = 1, \dots, m$). Specially, $p_i = 0$ means there is no coefficient in the *i*th equation. Let $C = (c_{11}, \dots, c_{1p_1}, \dots, c_{m1}, \dots, c_{mp_m})$ represent the vector consisting of all the empirical coefficients, and *M*(*C*) denote the mathematical models *M* with the coefficients *C*. Because the coefficient adaptation problem focuses only on the relationship between the coefficients *C* and the operating conditions *O*, we simplify Eq. (1) as:

$$Sim(M(C), O) \tag{3}$$

Let *Expo* denote the experimental data related to *O*, then we define the distance between the simulation results and experimental data specifically for *C* and *O* as $f_O(C)$ (which will be called the objective function from now on):

$$f_O(C) = |Sim(M(C), O) - Expo| \tag{4}$$

Here, we redefine the combined meaning of the absolute value sign and the minus sign, representing a feasible way of calculating how far the simulation results deviate from the experimental data. Let C_{Best_O} denote the best values of coefficients under the operating conditions *O*, then the formal description of coefficient adaptation problem can be given as:

$$C_{Best_O} = argmin[f_O(C)] \tag{5}$$

We assume that the best values of the coefficients will change with the operating conditions, which can be described by a mathematical equation. Let $C_{Best} = (c_1, \dots, c_r) \in \mathcal{C}$ denote the *r*-dimensional vector of all the coefficients, $O = (o_1, \dots, o_s) \in \mathcal{O}$ the *s*-dimensional vector consisting of *s* operating condition components, $\mathcal{C} \subset \mathbb{R}^r$, $\mathcal{O} \subset \mathbb{R}^s$, then the equation can be written as:

$$C_{Best} = g(O) \tag{6}$$

Here, *g*(*O*) is vector-valued with *r* components, and *g* represents a certain mapping rule from the domain \mathcal{O} to the domain \mathcal{C} .

If such equation(s) shown in Eq. (6) is acquired, tedious work of simulation and calibration with experimental data before determining the best values of coefficients can be simplified. To the best of our knowledge, there exists no theory that demonstrate the relationship between the best values of coefficients and the operating conditions. Our idea is to analyze the potential relationship and figure out the function *g* via an efficient and intelligent method based on a set of discrete points

$$\left\{ \left(O_i, C_{Best_{O_i}} \right) \middle| O_i \in \mathcal{O}, C_{Best_{O_i}} \in \mathcal{C}, i = 1, \dots, t \right\}$$

generated by Eq. (5). In this way, Eq. (6) acquired will have high congruency with Eq. (5), and for this reason, it can be the final instruction of configuring the empirical coefficients according to the operating conditions.

3. COEFFICIENT ADAPTATION MODEL FOR THE ZWART MODEL

In the present study, we considered the coefficient adaptation problem of the Zwart model based on the simulation of the quasi-steady cavitating flows around a two-dimensional NACA66 (MOD) hydrofoil. The mathematical models *M* involved were the continuity, the momentum equation for the liquid-vapour mixture, the volume fraction equation for the liquid phase, the cavitation model, and the turbulence model. For simplicity, we focused only on the empirical coefficients of the cavitation model and neglected those of other equations. In 3.1, 3.2 and 3.3, the mathematical models related are introduced first, and in 3.4 the definition of the coefficient adaptation model for the Zwart model is given.

3.1 Governing Equations

In this study, the multiphase flow was solved via the homogeneous equilibrium approach:

$$\frac{\partial \rho_m}{\partial t} + \frac{\partial (\rho_m u_j)}{\partial x_j} = 0 \quad (7)$$

$$\frac{\partial (\rho_m u_i)}{\partial t} + \frac{\partial (\rho_m u_i u_j)}{\partial x_j} = -\frac{\partial P}{\partial x_i} + \frac{\partial}{\partial x_j} \left[(\mu_m + \mu_t) \left(\frac{\partial u_i}{\partial x_j} + \frac{\partial u_j}{\partial x_i} \right) \right] \quad (8)$$

$$\frac{\partial \rho_l \alpha_l}{\partial t} + \frac{\partial (\rho_l \alpha_l u_j)}{\partial x_j} = \dot{m}^+ + \dot{m}^- \quad (9)$$

The above equations are, in order, the continuity, the momentum equation for the liquid-vapour mixture, and the volume fraction equation for the liquid phase. Phases are considered incompressible and all phases share the same velocity field. u_i and u_j (m/s) represent the components of time-averaged mixture velocity, P (Pa) the time-averaged pressure, ρ_m the density of the liquid-vapour mixture, ρ_l the liquid density, ρ_v the vapour density, α_l the liquid volume fraction, α_v the vapour volume fraction and $\alpha_l + \alpha_v = 1$, μ_m the dynamic viscosity of the liquid-vapour mixture, μ_l the liquid dynamic viscosity, μ_v the vapour dynamic viscosity, μ_t the turbulence viscosity, \dot{m}^+ the condensation rate, and \dot{m}^- the evaporation rate. The density and the dynamic viscosity of the liquid-vapour mixture are defined as:

$$\begin{cases} \rho_m = \rho_l \alpha_l + \rho_v \alpha_v \\ \mu_m = \mu_l \alpha_l + \mu_v \alpha_v \end{cases} \quad (10)$$

In order to close the set of Eqs. (7),(8),(9), the turbulence viscosity μ_t and the interphase mass transfer rate need to be modeled.

3.2 Turbulence Model

Cavitation flows are high Reynolds and high turbulent flows. In this study, the standard $k - \varepsilon$ turbulence model was adopted. In the literature, the standard $k - \varepsilon$ turbulence model performs well with simulating steady-state cavitating flows around the two-dimensional NACA66(MOD) hydrofoil. The transport equations of the turbulence kinetic energy k and the dissipation rate ε are as follows:

$$\frac{\partial (\rho_m k)}{\partial t} + \frac{\partial (\rho_m u_i k)}{\partial x_i} = p_k - \rho_m \varepsilon + \frac{\partial}{\partial x_i} \left[\left(\mu_m + \frac{\mu_t}{\sigma_k} \right) \frac{\partial k}{\partial x_i} \right] \quad (11)$$

$$\frac{\partial (\rho_m \varepsilon)}{\partial t} + \frac{\partial (\rho_m \varepsilon u_i)}{\partial x_i} = C_{1\varepsilon} \frac{\varepsilon}{k} p_k - C_{2\varepsilon} \rho_m \frac{\varepsilon^2}{k} + \frac{\partial}{\partial x_j} \left[\left(\mu_m + \frac{\mu_t}{\sigma_\varepsilon} \right) \frac{\partial \varepsilon}{\partial x_j} \right] \quad (12)$$

where μ_t represents the turbulent viscosity, p_k is the turbulent generation coefficient, $C_{1\varepsilon}$, $C_{2\varepsilon}$, σ_k and σ_ε are constants. μ_t is calculated as below:

$$\mu_t = \rho_m C_\mu \frac{k^2}{\varepsilon} \quad (13)$$

where C_μ is a constant. The values of the constants are as follows:

Table 1 Constants of the standard $k - \varepsilon$ model

$C_{1\varepsilon}$	$C_{2\varepsilon}$	C_μ	σ_k	σ_ε
1.44	1.92	0.09	1.0	1.3

To adapt to the Zwart model better, we modified μ_t according to (Philip J. Zwart 2004):

$$\mu_t = f(\rho) C_\mu \frac{k^2}{\varepsilon} \quad (14)$$

Where

$$f(\rho) = \rho_v + \left(\frac{\rho_v - \rho_m}{\rho_v - \rho_l} \right)^n (\rho_l - \rho_v) \quad (15)$$

3.3 Cavitation Model

The cavitation model used in this study was the Zwart model, which was derived from a simplified Rayleigh - Plesset equation (Brennen 2005):

$$\dot{m}^+ = F_c \frac{3\alpha_v \rho_v}{R_B} \sqrt{\frac{2}{3} \frac{P - P_v}{\rho_l}} \quad \text{if } P > P_v \quad (16)$$

$$\dot{m}^- = -F_e \frac{3\alpha_{nuc} (1 - \alpha_v) \rho_v}{R_B} \sqrt{\frac{2}{3} \frac{P_v - P}{\rho_l}} \quad \text{if } P < P_v \quad (17)$$

where P_v is the saturated vapour pressure, α_{nuc} is the nucleation site volume fraction, R_B is the radius of a nucleation site, F_c and F_e are two empirical coefficients for the condensation rate and the evaporation rate, respectively. In (Philip J. Zwart 2004), the default values of the above coefficients are given as: $\alpha_{nuc} = 5 \times 10^{-4}$, $R_B = 1 \times 10^{-6} m$, $F_c = 0.01$, $F_e = 50$. In literature, F_c and F_e are the calibration coefficients while the other two coefficients α_{nuc} and R_B are set by default (Morgut, Nobile, Bilu, and Scaron 2011). In our study, we only considered F_c and F_e , which directly control the cavitation process. Thus, C is expressed as $C = (F_c, F_e)$. All the other coefficients are set with default values.

3.4 Definition of Coefficient Adaptation Model for the Zwart Model

The coefficient adaptation model for the Zwart model contains two key modules: the optimization module and the prediction module. The optimization module calibrates the empirical coefficients under limited number of operating

conditions and transfers the best values of the coefficients accompanied with the corresponding operating conditions to the prediction module, which will then model the relationship between the best values of the coefficients and the operating conditions. In the present study, we considered \mathbf{O} as a vector consisting of three components: the angle of attack α of the NACA66(MOD) hydrofoil, the inlet velocity U_∞ and pressure P_∞ , namely $\mathbf{O} = (\alpha, U_\infty, P_\infty)$. The objective function $f_{\mathbf{O}}(\mathbf{C})$ was defined as the sum of the differences between the numerical values and the experimental values of the pressure coefficient, measured at 12 locations along the suction side of the NACA66(MOD) hydrofoil, for each couple of \mathbf{C} and \mathbf{O} .

$$f_{\mathbf{O}}(\mathbf{C}) = \sum_{i=1}^{12} |C_{PiSim_{\mathbf{O}}} - C_{PiExp_{\mathbf{O}}}| \quad (18)$$

In the above equation, $C_{PiSim_{\mathbf{O}}}$ and $C_{PiExp_{\mathbf{O}}}$ are the numerical value and the experimental value of the pressure coefficient at the i th location along the suction side of the hydrofoil under the operating condition \mathbf{O} , respectively. $C_{PiSim_{\mathbf{O}}}$ is calculated as:

$$C_{PiSim_{\mathbf{O}}} = \frac{P_i - P_{ref}}{\frac{1}{2} \rho_i U_\infty^2} \quad (19)$$

where P_i is the numerical value of the local pressure at the i th location along the suction side of the hydrofoil, P_{ref} is the reference pressure, $P_{ref} = P_\infty$.

Assume that there is a set of limited number of operating conditions with corresponding experimental data $\mathbb{O}_{Exp} = \{\mathbf{O}_1, \dots, \mathbf{O}_t\} \subset \mathbb{O}$. In the optimization module, all the elements in \mathbb{O}_{Exp} are processed by Eqs. (18) and (5) in order to get the set of optimization results $\mathbb{E} = \{(\mathbf{O}_i, \mathbf{C}_{Best_{\mathbf{O}_i}}) | \mathbf{O}_i \in \mathbb{O}, \mathbf{C}_{Best_{\mathbf{O}_i}} \in \mathbb{C}, i = 1, \dots, t\}$. We used $Opt()$ as the function to represent the optimization process:

$$\mathbb{E} = Opt(\mathbb{O}_{Exp}, \mathbf{C}) \quad (20)$$

Later, the prediction module will perform on \mathbb{E} to model the potential relationship between the best values of the coefficients $\mathbf{C} = (F_c, F_e)$ and the operating conditions $\mathbf{O} = (\alpha, U_\infty, P_\infty)$. Here, we neglected the interaction between F_c and F_e , and separately considered their relationship with α , U_∞ and P_∞ . Let M_{F_c} and M_{F_e} be the relationship models related to the two coefficients F_c and F_e respectively. We used $Train()$ as the function to represent the modeling process:

$$(M_{F_c}, M_{F_e}) = Train(\mathbb{E}) \quad (21)$$

Let F_{cBest} and F_{eBest} denote the best values of F_c and F_e , which can be predicted by M_{F_c} and M_{F_e} respectively:

$$\begin{cases} \hat{F}_{cBest} = M_1(\alpha, U_\infty, P_\infty) \\ \hat{F}_{eBest} = M_2(\alpha, U_\infty, P_\infty) \end{cases} \quad (22)$$

Equations (20) and (21) comprise the mathematical form of the coefficient adaptation model for the Zwart model. It should be noted that M_{F_c} and M_{F_e} can be trained and generated by different modeling methods, which can be treated as independent modules. In our study, we adopted one of the neural networks, the Radial Basis Function Neural Network(RBFNN) as the intelligent method to predict optimal coefficients. RBFNN has its outstanding advantages: It can approach any complicated nonlinear function relations and deal with the unanalyzable regularity in the system; It has good generalization ability and fast learning convergence speed. Thus, RBFNN has been successfully applied in time series analysis, pattern recognition, image processing, system modeling and other fields (Bellovin 2003; Lee and Ko 2009; Han, Chen, and Qiao 2011; Meng, Wu, Lu, and Toh 2002; Lu and Zhou 2009).

4. DESIGN AND IMPLEMENTATION OF COEFFICIENT ADAPTATION METHOD

As previously described, the coefficient adaptation model for the Zwart model contains the optimization module and the prediction module. The general framework is shown in Fig. 1. Firstly, the operating conditions and the corresponding experimental data are input to the whole system, and then the optimization module will generate an optimization case for each operating condition respectively. After that, the optimization module will create copies of the optimizer, which conducts the calibration of F_c and F_e for each optimization case. All the optimizers work in parallel and after all the optimization work is done, the optimization results will be collected and sent to the prediction module, which will build the relationship model to predict the optimal coefficients according to operating conditions.

The aim of coefficient optimization is to obtain the set of optimization results $\mathbb{E} = \{(\mathbf{O}_i, \mathbf{C}_{Best_{\mathbf{O}_i}}) | \mathbf{O}_i \in \mathbb{O}, \mathbf{C}_{Best_{\mathbf{O}_i}} \in \mathbb{C}, i = 1, \dots, t\}$ for modeling use. The optimizer in the optimization module applies the surrogate-based sequential approximate optimization (SAO) method to acquire the best values of the empirical coefficients. The SAO method introduces the approximate model technique to the process of optimization and adopts an effective approach of renewing the sampling points, which can remarkably reduce time cost and resources. For this reason, it has been widely used in complex engineering optimization. (Queipo, Haftka, Wei, Goel, Vaidyanathan, and Tucker 2005; Kleijnen 1986; Forrester and Keane 2009) We implemented the SAO method specifically for our research goal. The SAO method mainly consists of three parts: preconditioning, approximate modeling and renewing of sampling points. The process of the SAO method is shown in Fig. 2.

Preconditioning deals with the scale unification between the two design variables F_c and F_e , the

selection of the initial sampling points, namely the initial values of the design variables, and simulation at the sampling points, the aim of which is to calculate the values of the objective function based on numerical results and to prepare for the approximate modeling. We applied the Optimal Latin Hypercube Design (OLHD) method to conduct the optimal selection of the initial sampling points within the design space (Park 1994). The design space is expanded referring to (Morgut, Nobile, Bilu, and Scaron 2011):

$$\begin{cases} F_c \in [0.0001, 0.1] \\ F_e \in [5, 1000] \end{cases} \quad (23)$$

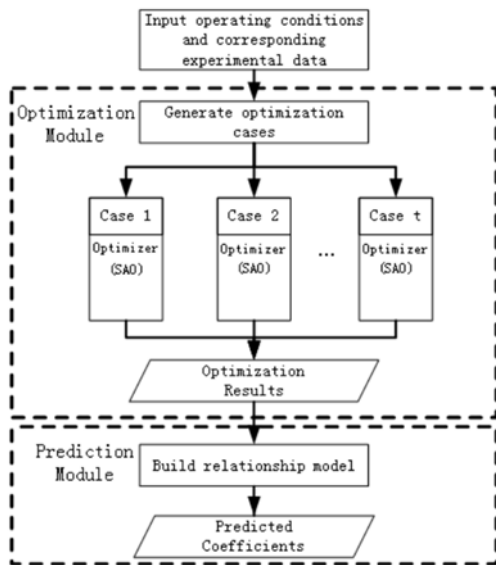


Fig. 1. General framework of the coefficient adaptation method.

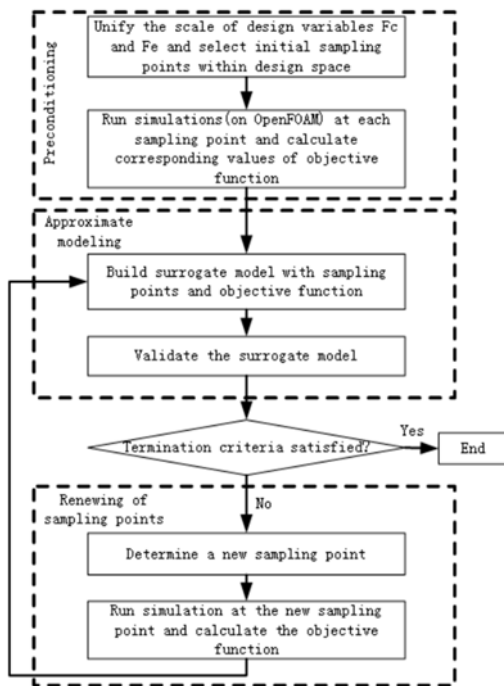


Fig. 2. Process of the SAO method.

Approximate modeling builds a surrogate model using fitting and interpolation based on radical basis function network (Thomson and Alexandra 1996) to predict the optimal values of F_c and F_e which combine to minimize the objective function. In order to validate the surrogate model, simulation will be performed with the predicted values of the coefficients to acquire the numerical results that can be used to calculate the objective function. If deviation between the calculated values and the predicted values of the objective function is undesirable, then the surrogate model will be reconstructed. Above steps will be repeated until the desirable surrogate model and the corresponding optimal values of the coefficients are found. Renewing of sampling points helps with the reconstruction of the surrogate model by adding a sampling point for building the surrogate model, using a Pareto front sampling method (Hughes 2003) to determine the new sampling point. The termination criteria is used to terminate the algorithm iteration process. A high-efficiency convergence criteria can drastically reduce unnecessary computational consumption. In our study, the two-step termination criteria was applied (Wang, Hu, Ma, Wu, and Zhang 2014):

1. If the new sampling point no longer contributes to the surrogate model updating.
2. If the new sampling point no longer contributes to the performance of the surrogate model at the optimal point.

The implementation of SAO approach was validated by solving Eq. (24) mentioned in (Wang, Hu, Ma, Wu, and Zhang 2014) before allocated into the optimizer. The evaluation results were similar to those given by (Wang, Hu, Ma, Wu, and Zhang 2014), which proved the effectiveness and efficiency of the implementation.

$$\begin{aligned} \min f(x) = & \left(4 - 2.1x_1^2 + x_1^4 / 3\right)x_1^2 + x_1x_2 \\ & + \left(4x_2^2 - 4\right)x_2^2 + x_1 + x_2 \end{aligned} \quad (24)$$

$$-2 \leq x_1, x_2 \leq 2$$

The optimizer will output the operating condition and the corresponding best values of the empirical coefficients after the iteration process terminates. Finally the prediction module will invoke the RBFNN module to build the relationship model after receiving the set of optimization results.

5. VALIDATION AND EVALUATION

5.1 Platform

Our tests were carried out on a HPC cluster situated in the State Key Laboratory of High Performance Computing, China. This hardware platform consists of hundreds of computing nodes connected via InfiniBand network with a total bandwidth of 40 Gb/s, and each computing node contains two hexcore 2.1 GHz Intel Xeon E5-2620 CPUs and 16 GB memory. The operating system of the cluster is Red Hat Enterprise Linux Server 6.5, on which OpenFOAM version 2.3.1 is installed. OpenFOAM

is an open source software for CFD which allows user-defined solvers and has good parallel computing capability. The solver used in our study was the `interPhaseChangeFoam`, which can solve multiphase flows. Because the `interPhaseChangeFoam` hasn't included the Zwart model, we programmed the Zwart model first and then implemented the coefficient adaptation platform for the Zwart model combined with OpenFOAM. In the prediction module, we invoked the RBFNN tools from MATLAB software to model the relationship between the optimal coefficients and the operating conditions.

5.2 Mesh and Case Setup

In the present study we considered the NACA66(MOD) hydrofoil with a camber ratio of $f/c = 0.020$, a NACA meanline of $a = 0.8$ and a thickness ratio of $t/c = 0.9$, where f is the maximum thickness, t the maximum camber and c the chord length of the hydrofoil section. The experimental data was from the measurements carried out by Shen and Dimotakis *et al.* in the High-Speed Water Tunnel of the California Institute of Technology (Dimotakis, Gaebler, Hamaguchi, Lang, and Shen 1987). In their experiments, the chord length of the hydrofoil model was $c = 0.150m$. During the experiments, leading edge sheet cavitation and midchord cavitation were investigated with the hydrofoil model placed at several angles of attack. In our study, we chose all the cases (28 in total) with definite experimental results under different combinations of the angle of attack α , the inflow velocity U_∞ and the inflow pressure P_∞ .

Rectangular domains were used in order to simulate the flows around the hydrofoil at different angles of attack. All the meshes were hexa-structured and generated using the ANSYS ICEM CFD 17.0 tool. It should be emphasized that although OpenFOAM can simulate two-dimensional flows, it can only support three-dimensional meshes. The original two-dimensional meshes from ICEM were converted to three-dimensional ones with small thickness by OpenFOAM's built-in tools. The boundary type of the additional two faces (Front and Back) of the three-dimensional meshes was set to "empty" in OpenFOAM, in order to achieve two-dimensional simulations. The computational domain and the imposed boundary conditions are shown in Fig. 3. The meshes were set as follows:

1. The Inlet and Outlet boundaries were placed respectively 3 chord lengths ahead of the leading edge, and 5 chord lengths behind the trailing edge. The Top and Bottom boundaries were placed 2.5 chord lengths from the hydrofoil.
2. Average values of y^+ on the hydrofoil surfaces were 30. y^+ was defined as $y^+ = (\mu_\tau y)/\nu$ where μ_τ was the friction velocity, y the normal distance from the wall, ν the kinematic viscosity.
3. On solid surfaces (Top, Bottom, Hydrofoil) the no-slip condition was applied.
4. The type of Front and Back boundaries was set to

"empty" in OpenFOAM.

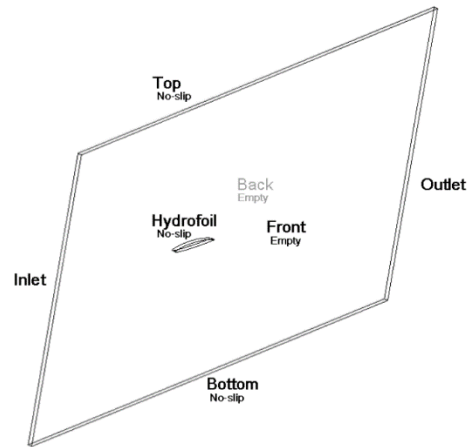


Fig. 3. Computational domain of the NACA66(MOD) hydrofoil and the imposed boundary conditions.

Before operating on the coefficient adaptation platform, the study of the influence of the mesh resolution was carried out in fully wetted (non-cavitating) conditions. This investigation was performed on the hydrofoils at all the angles of attack concerned in our study, by monitoring the influence of the progressively finer meshes on the lift coefficient C_L and the drag coefficient C_D . During the mesh refinement, the distances of the first nodes from the solid surfaces were kept unchanged, in order to perform a consistent mesh independence study. 48 processes for parallel simulation were allocated, which was also configured in the optimization module. C_L and C_D are defined as follows:

$$C_L = \frac{F_L}{(1/2)\rho U_\infty^2 S} \quad C_D = \frac{F_D}{(1/2)\rho U_\infty^2 S} \quad (25)$$

where $S = c \times d$ is the planar surface with d equal to the span. The span in our study was set to $d = 0.01m$, which was the same as the thickness of the meshes.

Table 2 Results of the mesh independence study carried out for NACA66(MOD) at $\alpha = 4^\circ$ and $Re = 2 \times 10^6$.

Mesh	Nodes	C_L	C_D
Coarse	41788	0.652	0.0017
Mid	97123	0.654	0.0018
Fine	186433	0.647	0.0019
Exp.		0.629	0.0018

Simulations under fully wetted conditions were conducted for all the angles of attack. Take the hydrofoil at $\alpha = 4^\circ$ as an example. The value of the free-stream velocity on the Inlet boundary was set to $U_\infty = 12.2m/s (Re = 2 \times 10^6)$ and the value of the static pressure on the Outlet boundary was set to $202650Pa$. Table 2 shows the results of the mesh independence study. From

the table, small differences among the three meshes can be seen as well as the acceptable difference from the experimental measurements. In Fig. 4 the pressure distributions along the surface of the hydrofoil computed from different meshes are very close to each other, and the suction side pressure distributions (the upper lines) for different meshes all compare favorably with the experimental measurements. Under the fully wetted condition, neither cavitation nor flow separation was found from these single-phase simulation results, which is in line with the experimental measurements. The same conclusion can be made in the mesh independence study of other angles of attack. Judging from better convergence compared with the coarse resolution meshes and less time cost compared with the fine resolution meshes, the mid resolution meshes were chosen in the following study. Figure 5 shows the mid resolution mesh around the NACA66(MOD) hydrofoil at $\alpha = 4^\circ$ and the close view of the leading edge region.

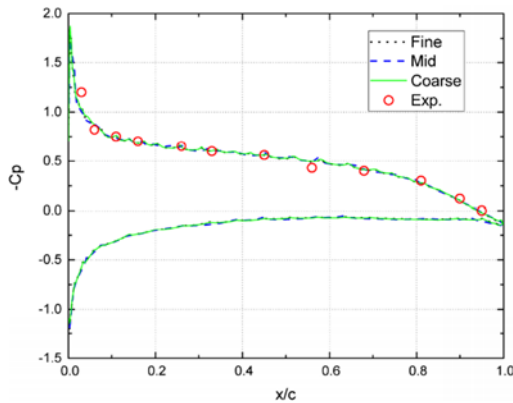


Fig. 4. Pressure distributions along the suction side (the upper lines) and the pressure side (the lower lines) of the NACA66(MOD) hydrofoil, for different mesh resolution levels at non cavitating flow conditions and at $\alpha = 4^\circ$, $Re = 2 \times 10^6$.

In simulating cavitating flows, we had, for each case and the corresponding computational mesh, the following settings besides those mentioned in mesh resolution study:

1. The value of the free-stream velocity on the Inlet boundary and the value of the static pressure on the Outlet boundary were set respectively equal to the U_∞ and P_∞ corresponding to each case. Initial water and vapour volume fractions were set to 1 and 0, respectively.
2. In all the simulations the water and vapour density were kept constant and equal to $\rho_l = 997\text{kg/m}^3$ and $\rho_v = 0.02308\text{kg/m}^3$. Assuming a turbulence intensity of 1%, the turbulent kinetic energy k and the turbulent dissipation rate ε were set equal to $k = 0.0233\text{m}^2/\text{s}^2$ and $\varepsilon = 0.1837\text{m}^2/\text{s}^3$. The saturated vapour pressure of water was $P_v = 3169\text{Pa}$.

5.3 Implementary Methodology

The aim of our tests was to validate the coefficient adaptation method for the Zwart model. After receiving the input of the operating conditions and experimental data of the 28 cases, the coefficient adaptation platform will generate and configure optimization cases on OpenFOAM as mentioned in 5.2, and activate the optimization module to perform parallel optimization work, whose results will be sent to the prediction module. In the prediction module, the optimization results of 3/4 of the cases were chosen randomly (covering all the angles of attack) as the training set to build the relationship model. The rest 1/4 cases (which will be called the test cases from now on) were used for subsequent validation of the model. For each test case, the best values of the coefficients $\mathbf{C}_{predicted_i} = (F_{c_{predicted_i}}, F_{e_{predicted_i}})$ with $\mathbf{O}_i = (\alpha_i, U_{\infty_i}, P_{\infty_i}) (i = 1, \dots, 7)$ according to the relationship model were predicted.

We used the following equation to evaluate the predicted values of the coefficients:

$$Err_{predicted} = \frac{1}{7} \sum_{i=1}^7 \frac{f_o(\mathbf{C}_{predicted_i}) - f_o(\mathbf{C}_{Best_i})}{f_o(\mathbf{C}_{Best_i})} \quad (26)$$

The smaller $Err_{predicted}$ is the closer to the best simulation results, thus the more consistent with the experimental data. Moreover, we tested the default values in (Philip J. Zwart 2004) and the tuned values in (Morgut, Nobile, Bilu, and Scaron 2011).

We replaced $\mathbf{C}_{predicted_i}$ in Eq. (26) with $\mathbf{C}_{Default_i} = (0.01, 50)$ and $\mathbf{C}_{Morgut_i} = (0.03, 300)$ respectively, and compared the results $Err_{Default}$ and Err_{Morgut} with $Err_{predicted}$.

5.4 Results and Discussion

The optimization results of the 28 cases yielded from the optimization module are shown in Table 3. $\mathbf{C}_{Best} = (F_{c_{Best}}, F_{e_{Best}})$ denotes the best values of the empirical coefficients. The cavitation number σ in Table 3 is calculated as:

$$\sigma = \frac{P_\infty - P_v}{\frac{1}{2} \rho_l U_\infty^2} \quad (27)$$

The number of iterations and mean CPU time in the SAO approach for each case are shown in Fig. 6. It is possible to see the efficiency and stable performance of the SAO approach from the figure. In this study, the number of iterations went from 128 to 185. It presents similar level of efficiency to the literature (Wang, Hu, Ma, Wu, and Zhang 2014). By allocating 48 processes for simulation during each single iteration, the mean CPU time was kept in the range of 6000 to 9000 seconds. The optimization results were collected after all the cases were done, and thus there would be a waste of waiting time. As the iterations and mean CPU time among the cases were relatively close, the waiting

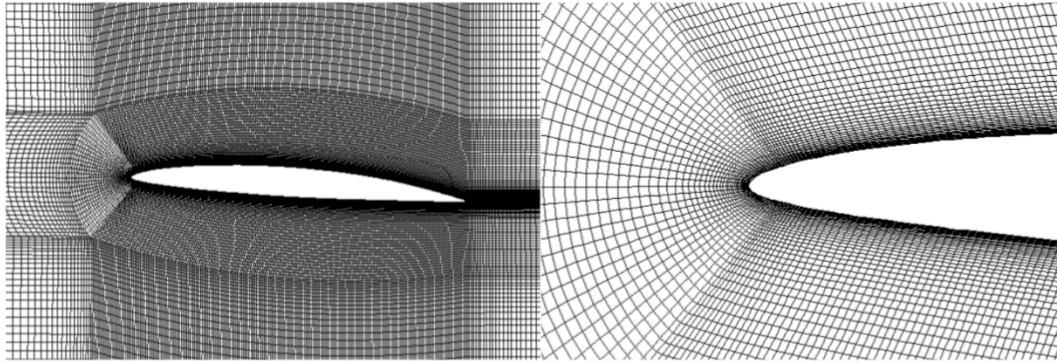


Fig. 5. Mid resolution mesh around NACA66(MOD) at the angle of attack of $\alpha=4^\circ$; large view(left), close view(right).

Table 3 Optimization results corresponding to all the 28 cases. The cases labeled M are for modeling use while those labeled V are for validation

No.	σ	$\alpha(^{\circ})$	$U_{\infty}(m/s)$	$P_{\infty}(Pa)$	F_{cBest}	F_{eBest}	Label
1	0.45	1	18.18	77290.23	0.0845	812.82	M
2	0.42	1	18.20	73153.37	0.0556	889.44	V
3	0.38	1	18.25	66396.51	0.0351	802.73	M
4	0.35	1	18.30	61501.23	0.0739	778.87	M
5	0.34	1	18.28	59708.6	0.0688	945.30	M
6	0.64	2	9.13	29854.3	0.0847	870.77	M
7	0.55	2	9.12	26062.18	0.0640	735.13	V
8	0.51	2	9.16	24545.33	0.0357	400.27	M
9	0.48	2	9.19	23235.33	0.0171	583.71	M
10	1.24	3	17.93	201258	0.0595	879.68	M
11	1.12	3	8.94	47780.67	0.0426	833.48	V
12	1.71	4	12.01	125898.3	0.0908	945.28	M
13	1.12	4	12.03	83978.14	0.0411	710.92	M
14	0.99	4	12.01	74601.27	0.0598	868.62	M
15	0.91	4	12.01	68327.04	0.0817	618.40	V
16	0.84	4	12.00	63569.66	0.0778	889.44	M
17	0.77	4	12.05	58536.49	0.0533	745.05	M
18	1.03	4	8.06	36542.21	0.0516	611.19	M
19	0.94	4	8.10	33991.15	0.0767	303.46	V
20	1.01	4	18.14	168507.9	0.0394	493.41	M
21	0.95	4	17.88	155201	0.0880	408.05	M
22	0.89	4	17.89	144927.8	0.0319	682.63	M
23	3.12	6	11.98	226354.9	0.0963	817.99	M
24	1.82	6	11.95	132448.3	0.0124	895.19	M
25	1.48	6	12.00	109764.5	0.0652	926.00	V
26	1.25	6	12.03	93561.85	0.0852	592.29	M
27	1.13	6	12.04	85012.35	0.0868	655.62	M
28	0.98	6	12.08	74739.17	0.0228	954.53	V

time was accept-able compared to the total CPU time cost in the optimization module. An example of the iterative convergence is demonstrated in Fig. 7. It presents the convergence curve of the objective function in Case 15. As is shown in the figure, the minimum of the objective function, which corresponds to the optimal values of the empirical coefficients, is found after 144 iterations. Moreover,

the accuracy of the optimization approach can be seen in Figs. 8 and 9, by comparing the best simulation results with the experimental data.

21 sets of optimization results were randomly chosen (covering all the angles of attack) as the input to the RBFNN(labeled M in Table 3) to build the relationship model. The predicted optimal coefficients by the relationship model $C_{Predicted} =$

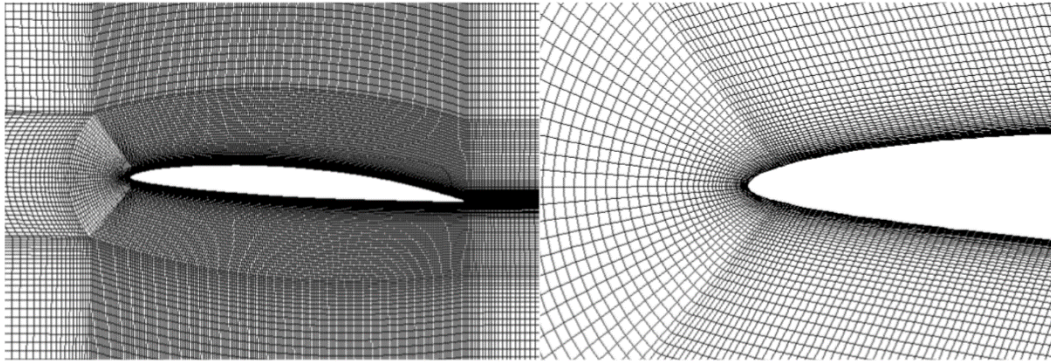


Fig. 5. Mid resolution mesh around NACA66(MOD) at the angle of attack of $\alpha=4^\circ$; large view(left), close view(right).

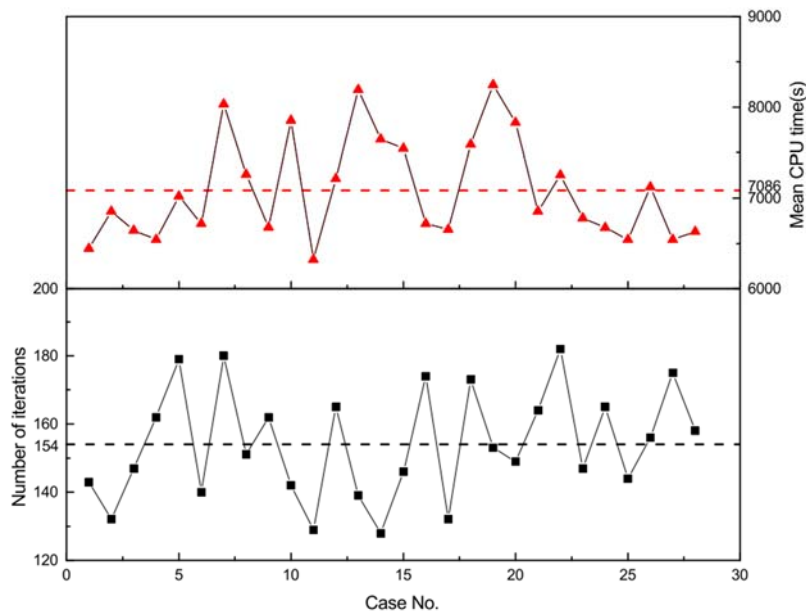


Fig. 6. Number of iterations (bottom) and mean CPU time (top) in the SAO approach for each case. The dash lines represent the average of the number of iterations and the average of the mean CPU time, respectively.

($F_{cPredicted}$, $F_{ePredicted}$) of the 7 test cases (labeled V in Table 3) are shown in Table 4. For each test case, simulations with C_{Best} , $C_{Default}$, C_{Morgut} and $C_{Predicted}$ respectively were carried out. With the simulation results we calculated the corresponding values of the objective function $fo(C)$, as shown in Table 5. Preliminarily we can see the predicted values are better than the default values and the Morgut values in overall.

Table 4 Predicted values of F_c and F_e for the test cases. The number of the case is in agreement with Table 3

No.	σ	$\alpha(^{\circ})$	$F_{cPredicted}$	$F_{ePredicted}$
2	0.42	1	0.0717	866.41
7	0.55	2	0.0433	618.65
13	1.12	4	0.0763	878.00
15	0.91	4	0.0702	809.41
19	0.94	4	0.0459	644.57
25	1.48	6	0.0699	701.28
28	0.98	6	0.0647	656.97

Table 5 Objective function calculated from the simulation results of the test cases with respectively four pairs of empirical coefficients

No.	Best	Default	Morgut	Predicted
2	0.764	0.774	0.785	0.787
7	0.124	0.237	0.238	0.157
13	0.188	0.237	0.238	0.206
15	0.285	0.298	0.302	0.293
19	0.282	0.309	0.301	0.298
25	0.477	0.499	0.493	0.499
28	1.238	1.292	1.284	1.239

Further observation of the pressure distributions along the surface of the hydrofoil is demonstrated in Fig. 8, and the cavitation patterns in Fig. 9. From the results given in Fig. 8, it seems that the pressure distributions along the pressure side (the lower lines) computed from different pairs of coefficient values are quite close to each other, but the suction side pressure distributions are obviously different. It can be concluded that the condensation and the

evaporation coefficients mainly influence the low-pressure area where cavitation occurs. In Case 2, midchord cavitation is observed over the hydrofoil at $\alpha = 1^\circ$, and that the lengths of cavity obtained with $C_{Default}$, C_{Morgut} and $C_{Predicted}$ are close to one another and are all much larger than that obtained with C_{Best} . It should be noted that even the best simulation results differ much from the experimental measurements. In Case 7 leading edge sheet cavitation at $\alpha = 2^\circ$ is shown. Compared with $C_{Default}$ and C_{Morgut} , the cavity length obtained with $C_{Predicted}$ is shorter and closer to that obtained with C_{Best} , and the suction side pressure coefficients are in better agreement with experimental measurements. Case 11, 15, and 19 show leading edge cavitation at $\alpha = 4^\circ$. In Case 11 the effects of all the pairs of coefficients are quite similar and agree well with the experimental measurements. In Case 15 the cavity length obtained with $C_{Predicted}$ is smaller and the suction side distributions agree better with experimental measurements, compared with $C_{Default}$ or C_{Morgut} . In Case 19, all the pairs of empirical coefficients have almost the same effect on the cavity pattern and the suction side pressure coefficients, with a small difference in the prediction of pressure at the end of the cavity. Case 25 and 28 show leading edge sheet cavitation at $\alpha = 6^\circ$. In Case 25 compared with $C_{Default}$ and C_{Morgut} , the cavity length obtained with $C_{Predicted}$ is closer to experimental measurements, but the prediction of pressure at the end of the cavity is less accurate. In Case 28 the effects of all the pairs of coefficients differ much from the experimental measurements, but we still can see $C_{Predicted}$ performs better than $C_{Default}$ or C_{Morgut} . In general, we can conclude that $C_{Predicted}$ is better than $C_{Default}$ and C_{Morgut} .

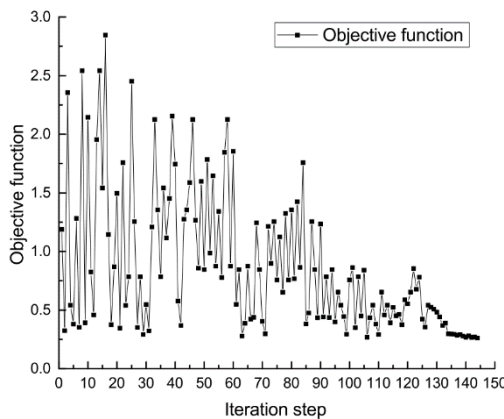


Fig. 7. Iterative convergence curve of the objective function of Case 15.

Table 6 Evaluation of $C_{Default}$, C_{Morgut} and $C_{Predicted}$

$Err_{Default}$	Err_{Morgut}	$Err_{Predicted}$
0.318	0.319	0.194

With Table 5 $Err_{Default}$, Err_{Morgut} and $Err_{Predicted}$ were calculated, as shown in Table 6. We can see $Err_{Default}$ and Err_{Morgut} are quite close to each other, indicating that the default values of the empirical coefficients result in similar accuracy with the

Morgut values. Moreover, compared with the constant values, that is, the default values and the Morgut values, the predicted values of the empirical coefficients increase the simulation accuracy by about 12% in average.

The overall results indicate that it is effective to use the coefficient adaptation method to solve the coefficient adaptation problem for the Zwart model and guide the configuration of the empirical coefficients under different operating conditions.

6. CONCLUSION

The coefficient adaptation problem is often encountered in CFD simulations. The accuracy of the simulation results depends much on the empirical coefficients of mathematical models. In literature, constant values of empirical coefficients are applied regardless of the operating conditions, and thus they cannot meet the needs of all operating conditions with good performance. Cavitation simulation is a typical application of CFD. Many modeling methods have been proposed to simulate cavitating flows in many cases. A widely used method is to solve RANS (Reynolds Averaged Navier Stokes) equations with an additional transport equation including the cavitation model which describes the variation of the volume fraction of the liquid phase. In cavitation simulations, researchers have proposed methods of obtaining the best values of the empirical coefficients of the cavitation model. However, these methods can only acquire constant values which aren't adaptive to all the operating conditions. In our present study, we focused on the Zwart model and carried out research into the prediction of the best values of empirical coefficients, considering quasi-steady cavitating flows around a two-dimensional NACA66(MOD) hydrofoil. The main contributions of this paper are summarized as follows:

1. For the first time, we gave a formal description of the coefficient adaptation problem and solution, and put forward the coefficient adaptation model and corresponding method including two key modules: the optimization module and the prediction module, which could model the relationship between the optimal coefficients of the CFD model and the operating conditions based on existed experimental measurements.
2. We designed and implemented the coefficient adaptation platform for the Zwart model through the method mentioned above, combining the open source software OpenFOAM. Then we performed optimization of the condensation coefficient F_c and the evaporation coefficient F_e of the Zwart model and validated the predicted optimal coefficients on the platform.
3. The overall results indicate that our method can effectively solve the coefficient adaptation problem of the Zwart model. The predicted coefficient values result in an

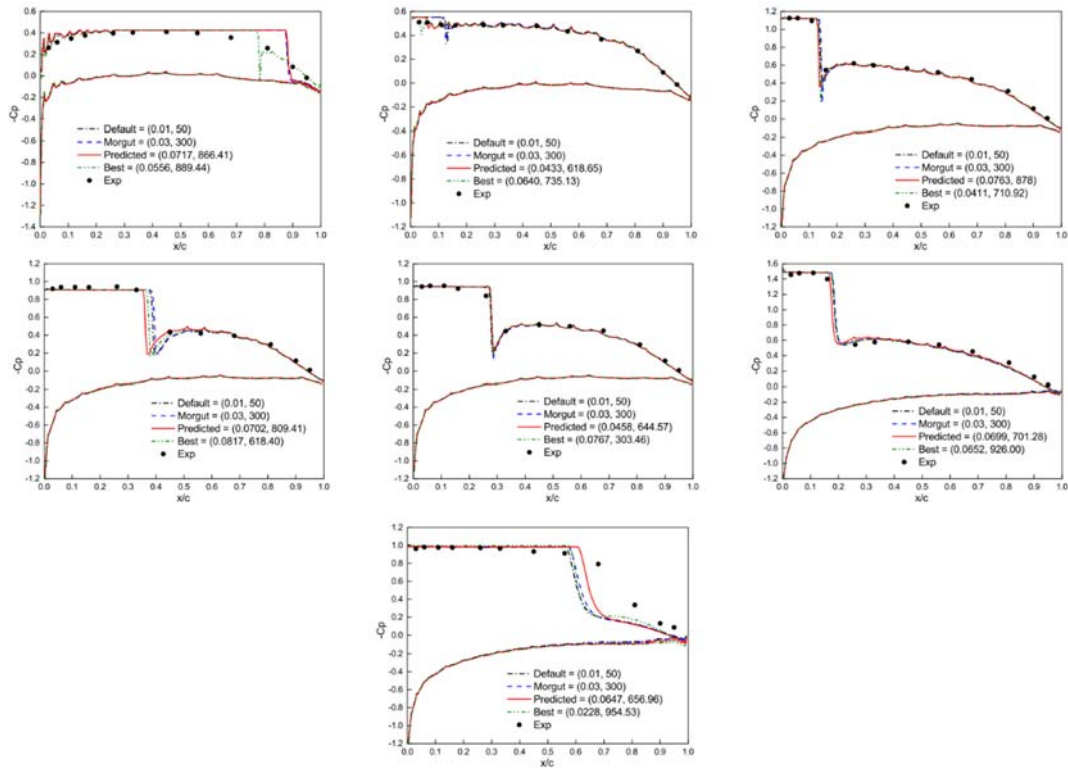


Fig. 8. Comparison of pressure distributions along the suction side(the upper lines) and the pressure side(the lower lines) of the NACA66(MOD) hydrofoil resulting from different pairs of empirical coefficients in the test cases.

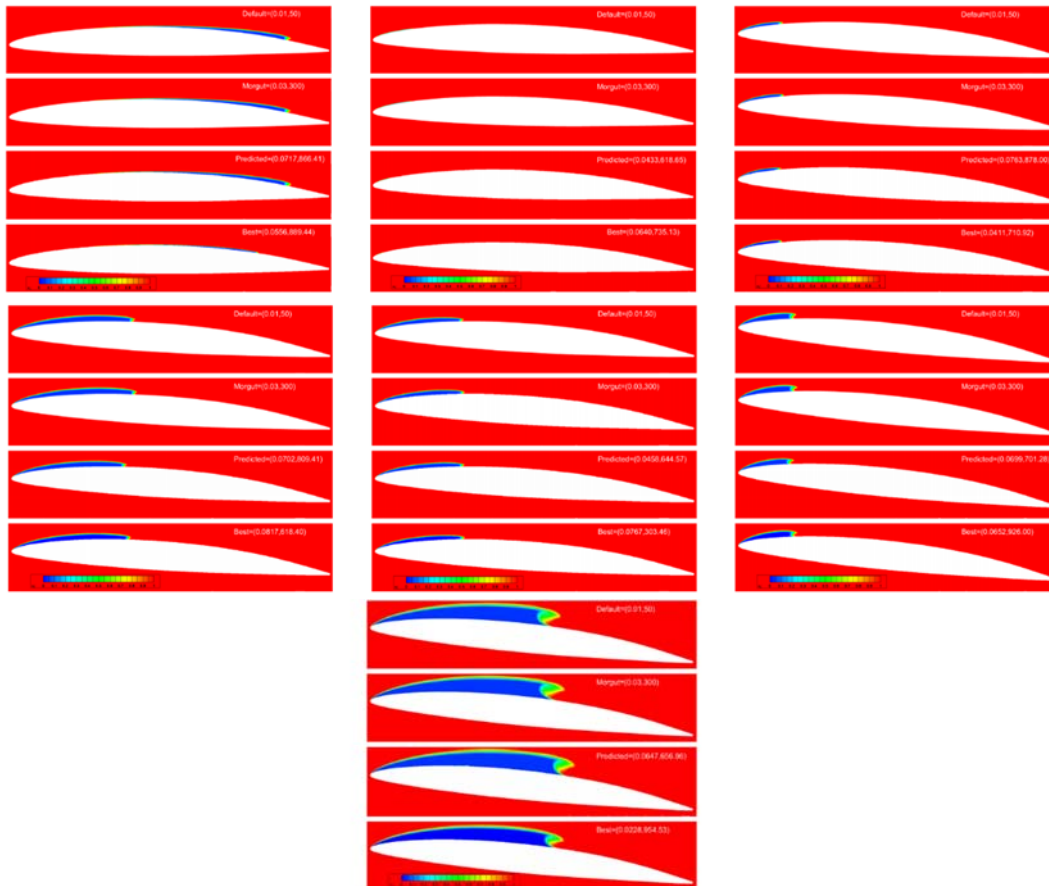


Fig. 9. Cavitation patterns resulting from different pairs of empirical coefficients (in order $C_{Default}$, C_{Morgut} , $C_{Predicted}$ and C_{Best}) in the test cases. The color scale shows different values of water volume fraction α_w .

increase of accuracy by 12% in average, compared with the default values (Philip J. Zwart 2004) and the tuned values given in (Morgut, Nobile, Bilu, and Scaron 2011).

We believe that the proposed method could be very useful in adaptively configuring the empirical coefficients of present, and also future, mathematical models in practical uses.

ACKNOWLEDGMENTS

The authors declare that there is no conflict of interest regarding the publication of this paper. The authors would like to thank the Key Research and Development Plan of Ministry of Science and Technology (Grant no. 2016YFB0201301) and the Science Challenge Program of CAEP (no. JCKY2016212A502 and TZ2016002) for funding.

REFERENCES

- Bellovin, S. (2003). Icmp traceback message. *Internet Draft, draft-ietf-itrace-04.txt*.
- Brennen, C. E. (1995). *Cavitation and bubble dynamics*. Oxford University Press.
- Brennen, C. E. (2005). *Fundamentals of Multiphase Flow*. Cambridge University Press.
- Dimotakis, P. E., H. F. Gaebler, H. T. Hamaguchi, D. B. Lang, and Y. T. Shen (1987). Two-dimensional naca 66(mod) hydrofoil high speed water tunnel tests. *California Institute of Technology*.
- Forrester, A. I. J. and A. J. Keane (2009). Recent advances in surrogate-based optimization. *Progress in Aerospace Sciences* 45(1), 50–79.
- Franc, J. P. and J. M. Michel (2005). Fundamentals of cavitation. *Fluid Mechanics and Its Applications* 76(11), 1–46.
- Hagar Alm, E., Y. S. Zhang, and E. Medhat (2012). A computational study of cavitation model validity using a new quantitative criterion. *Chinese Physics Letters* 29(6), 064703–1920.
- Han, H. G., Q. L. Chen, and J. F. Qiao (2011). An efficient self-organizing rbf neural network for water quality prediction. *Neural Networks* 24(7), 717–725.
- Hirschi, R., P. Dupont, F. Avellan, J. N. Favre, J. F. Guelich, W. Handloser, and E. Parkinson (1998). Centrifugal pump performance drop due to leading edge cavitation: Numerical predictions compared with model tests. *Journal of Fluids Engineering* 120(4), 705–711.
- Hou-lin, Wang, Deng-hao, Wei-min, and Ming-gao (2012). Research of inner flow in a double blades pump based on openfoam. *Journal of Hydrodynamics, Ser. B* 24(2), 226–234.
- Hughes, E. J. (2003). Multiple single objective pareto sampling. In *Evolutionary Computation, 2003. CEC '03. The 2003 Congress on*, pp. 2678–2684 Vol.4.
- Kleijnen, J. P. C. (1986). *Statistical tools for simulation practitioners*. Marcel Dekker, Inc.
- Kunz, R. F., D. A. Boger, D. R. Stinebring, T. S. Chyczewski, J. W. Lindau, H. J. Gibeling, S. Venkateswaran, and T. R. Govindan (2000). A preconditioned navierstokes method for two-phase flows with application to cavitation prediction. *Computers and Fluids* 29(8), 849–875.
- Launder, B. E. and D. B. Spalding (1974). The numerical computation of turbulent flows. *Computer Methods in Applied Mechanics and Engineering* 3(2), 269–289.
- Lee, C. M. and C. N. Ko (2009). Time series prediction using rbf neural networks with a nonlinear time-varying evolution pso algorithm. *Neurocomputing* 73(1), 449–460.
- Liu, H. L., J. Wang, Y. Wang, H. Zhang, and H. Huang (2014). Influence of the empirical coefficients of cavitation model on predicting cavitating flow in the centrifugal pump. *International Journal of Naval Architecture and Ocean Engineering* 6(1), 119–131.
- Lu, N. and J. Zhou (2009). Particle swarm optimization-based rbf neural network load forecasting model. *IEEE*, 1 – 4.
- Meng, J. E., S. Wu, J. Lu, and H. L. Toh (2002). Face recognition with radial basis function rbf neural network. *IEEE Transactions on Neural Networks* 13(3), 697–710.
- Merkle, C. L., J. Feng, and P. E. O. Buelow (1998). Computational modeling of the dynamics of sheet cavitation.
- Morgut, M., E. Nobile, Bilu, and I. Scaron (2011). Comparison of mass transfer models for the numerical prediction of sheet cavitation around a hydrofoil. *International Journal of Multiphase Flow* 37(6), 620–626.
- Park, J. S. (1994). Optimal latin-hypercube designs for computer experiments. *Journal of Statistical Planning and Inference* 39(1), 95–111.
- Philip J. Zwart, Andrew G. Gerber, T. B. (2004). A two-phase flow model for predicting cavitation dynamics. In *Icmf-2004, International Conference on Multiphase Flow*.
- Queipo, N. V., R. T. Haftka, S. Wei, T. Goel, R. Vaidyanathan, and P. K. Tucker (2005). Surrogate-based analysis and optimization. *Progress in Aerospace Sciences* 41(1), 1–28.
- Schnerr, G. H., S. J. (2001). Physical and numerical modeling of unsteady cavitation dynamics. In *Proceedings ICMF 2001- 4th International Conference on Multiphase Flow, New Orleans, USA, May 27 - June 1*.

- Senocak, I. and S. Wei (2004). Interfacial dynamics-based modelling of turbulent cavitating flows, part-1: Model development and steady-state computations. *Frontiers in Public Health* 2(2), 141.
- Senocak, I. and W. Shyy (2002). Evaluation of cavitation models for navier-stokes computations. *American Society of Mechanical Engineers Fluids Engineering Division Fed.*
- Singhal, A. K., M. M. Athavale, H. Li, and Y. Jiang (2002). Mathematical basis and validation of the full cavitation model. *Journal of Fluids Engineering* 124(3), 617–624.
- Thompson and R. C. Alexandra (1996). Radical basis function modelling and prediction of time series. *Acs Nano* 6(10), 8857–8867.
- Tushar, G., T. Siddharth, R. T. Haftka, S. Wei, and J. Zhao (2010). Surrogate model-based strategy for cryogenic cavitation model validation and sensitivity evaluation. *International Journal for Numerical Methods in Fluids* 58(9), 969–1007.
- Wang, D., F. Hu, Z. Ma, Z. Wu, and W. Zhang (2014). A cad/cae integrated framework for structural design optimization using sequential approximation optimization. *Advances in Engineering Software* 76(3), 56–68.
- Wilcox, D. C. (1993). Turbulence modeling for cfd. *Dcw Industries La Canada California Usa*, 363–367.
- Zhao, X., B. Huang, T. Chen, G. Wang, D. Gao, and J. Zhao (2017). Numerical simulations and surrogate-based optimization of cavitation performance for an aviation fuel pump. *Journal of Mechanical Science and Technology* 31(2), 705–716.